

# Mean-field effects on particle and antiparticle elliptic flows in the beam-energy scan program at RHIC

Jun Xu,<sup>1,\*</sup> Che Ming Ko,<sup>2</sup> Feng Li,<sup>2</sup> Taesoo Song,<sup>3</sup> and He Liu<sup>1</sup>

<sup>1</sup>*Shanghai Institute of Applied Physics, Chinese Academy of Sciences, Shanghai 201800, China*

<sup>2</sup>*Cyclotron Institute and Department of Physics and Astronomy,  
Texas A&M University, College Station, Texas 77843, USA*

<sup>3</sup>*Frankfurt Institut for Advanced Studies and Institute for Theoretical Physics,  
Johann Wolfgang Goethe Universitat, Frankfurt am Main, Germany*

(Dated: August 3, 2021)

The elliptic flow splitting between particles and their antiparticles has recently been observed by the STAR Collaboration in the beam-energy scan program at the Relativistic Heavy Ion Collider. In studies based on transport models, we have found that this splitting can be explained by the different mean-field potentials acting on particles and their antiparticles in the produced baryon-rich matter. In particular, we have shown that the experimentally measured relative elliptic flow difference can help constrain the vector coupling constant in the Nambu-Jona-Lasinio model used in describing the partonic stage of heavy-ion collisions. This information is useful for locating the critical point in the QCD phase diagram and thus understanding the phase structure of QCD.

PACS numbers: 25.75.-q, 12.38.Mh, 24.10.Lx, 24.85.+p

## I. INTRODUCTION

The main goal of experiments on relativistic heavy-ion collisions is to study the hadron-quark phase transition or the QCD phase structure. At top energies of the Relativistic Heavy Ion Collider (RHIC) and the Large Hadron Collider (LHC), the produced quark-gluon plasma (QGP) is essentially baryon free and the phase transition is thus a smooth crossover according to results from the lattice QCD calculations [1–3]. On the other hand, studies based on various theoretical models have predicted that the hadron-quark phase transition becomes a first-order one at large baryon chemical potential [4–7]. A critical point is thus expected to exist between the smooth crossover and the first-order phase transition. To search for its signature, experiments under the beam-energy scan (BES) program have recently been carried out at RHIC. Although there is no definitive conclusion on the location of the QCD critical point, some interesting phenomena different from those observed in heavy-ion collisions at much higher energies have been observed [8, 9], such as the weakening in the charge separation, the net proton number fluctuation, the fluctuation of  $p/\pi$  and  $K/\pi$  ratios, the monotonic decrease of the freeze-out eccentricity with increasing beam energy from the Hanbury-Brown Twiss analysis, the larger nuclear modification factor for high-transverse-momentum particles than in collisions at higher energies, and the splitting of the direct flow and elliptic flow between particles and their antiparticles.

The observed elliptic flow ( $v_2$ ) splitting between particles and their antiparticles [10] in the BES program at RHIC, which obviously indicates the break down of

the number of constituent quark scaling established at higher collision energies [11], has attracted much attention. Various explanations have been suggested for understanding this phenomenon. It was shown in Ref. [12] that the chiral magnetic wave induced by the strong magnetic field from non-central heavy-ion collisions could lead to a charge quadrupole moment in the participant region, which would then result in a larger  $v_2$  for positively charged particles than negatively charged ones, especially for charged pions due to their similar final-state interactions. Also, the different  $v_2$  between particles and their antiparticles has been attributed to different  $v_2$  of produced and transported particles [13], different rapidity distributions for quarks and antiquarks [14], and the conservation of baryon charge, strangeness, and isospin [15].

On the other hand, we have shown in our recent studies [16–20] that the observed  $v_2$  splitting can be explained by the different mean-field potentials acting on particles and their antiparticles. The effect of the mean-field potential or the nuclear matter equation of state on the elliptic flow was already known in heavy ion collisions at SIS energies of the order 1 AGeV [21]. At this energy, the expansion of the hot participant matter is blocked by the cold spectator matter, resulting in the emission of more particles out of the reaction plane and thus a negative  $v_2$ . A more repulsive mean-field potential leads to a fast expansion of the participant matter, thus a stronger blocking effect and an even more negative  $v_2$ . This becomes different in relativistic heavy-ion collisions where the blocking effect is absent as the spectator matter quickly moves away from the participant region. As a result, particles with repulsive potentials are more likely to leave the system, while those with attractive potentials are more likely trapped in the system. For the case of a positive eccentricity of the participant region in non-central collisions, the  $v_2$  is then enhanced for particles with repulsive potentials and suppressed for those with

---

\*Electronic address: xujun@sinap.ac.cn

attractive potentials. In the baryon-rich matter formed in heavy-ion collisions at  $\sqrt{s_{NN}} = 7.7 \sim 39$  GeV in the BES program at RHIC, particles usually have repulsive or less attractive potentials compared to the strong attractive potentials for their antiparticles, and the difference becomes smaller with decreasing net baryon density at higher collision energies. This qualitatively explains the observed decreasing  $v_2$  splitting with increasing beam energy.

This paper is organized as follows. In Sec. II, we briefly review the physics contents of a multiphase transport model based on which our studies were carried out. The hadronic potentials and the partonic potentials as well as their effects on  $v_2$  splitting between particles and antiparticles are discussed in Sec. III and Sec. IV, respectively. Results with the inclusion of both potentials are shown in Sec. V. Finally, conclusions and outlook are given in Sec. VI.

## II. THE AMPT MODEL

Our study of the mean-field effects on  $v_2$  splitting between particles and their antiparticles were based on a multiphase transport (AMPT) model [22]. To properly describe the relative contributions of the partonic phase and the hadronic phase on the final elliptic flow of hadrons, we use the string melting version, which converts hadrons produced from initial collisions into their valence quarks and antiquarks, and was shown to successfully reproduce the charged particle multiplicity, the collective flow, and the dihadron correlations at both RHIC and LHC [23].

The initial conditions in the AMPT model are obtained from the heavy-ion jet interaction generator (HIJING) model [24], where both soft and hard scatterings are included by using the Monte Carlo Glauber model with nuclear shadowing effects. In the string melting version, the interaction in the partonic phase is described by parton-parton elastic scatterings based on the Zhang's parton cascade (ZPC) model [25]. After the freeze-out of partons, a spatial coalescence model is used to describe the hadronization process with the hadron species determined by the flavor and invariant mass of its constituent quarks and/or antiquarks. The evolution of resulting hadronic phase is described by a relativistic transport (ART) [26], which has been generalized to include both baryon-antibaryon annihilations to two-meson states and their inverse processes [22]. The cross sections for the former are determined by the branching ratios for producing corresponding number of pions according to the phase space considerations, while the cross sections for the latter are based on the detailed balance relations. For heavy ion collisions at top energies at RHIC and LHC, the mean-field potentials for particles and their antiparticles are not included in either ZPC or ART as they are less important than partonic and hadronic scatterings on the collision dynamics [23]. In Refs. [16–20], the AMPT

model was extended to include mean-field potentials in the hadronic phase and the partonic phase in order to study heavy ion collisions at energies carried out in the BES program.

## III. EFFECTS OF HADRONIC POTENTIALS

For nucleon and antinucleon potentials, they can be calculated from the relativistic mean-field model used in Ref. [27] to describe the properties of nuclear matter, i.e.,

$$U_{N,\bar{N}}(\rho_B, \rho_{\bar{B}}) = \Sigma_s(\rho_B, \rho_{\bar{B}}) \pm \Sigma_v(\rho_B, \rho_{\bar{B}}), \quad (1)$$

where  $\Sigma_s(\rho_B, \rho_{\bar{B}})$  and  $\Sigma_v(\rho_B, \rho_{\bar{B}})$  are the nucleon scalar and vector self-energies in a hadronic matter of baryon density  $\rho_B$  and antibaryon density  $\rho_{\bar{B}}$ , with "+" for nucleons and "-" for antinucleons, respectively. Nucleons and antinucleons contribute both positively to  $\Sigma_s$  but positively and negatively to  $\Sigma_v$ , respectively, as a result of the  $G$ -parity invariance. The potentials for strange baryons and antibaryons are reduced relative to those of nucleons and antinucleons according to the ratios of their light quark numbers.

The kaon and antikaon potentials in the nuclear medium are also taken from Ref. [27] based on the chiral effective Lagrangian, that is  $U_{K,\bar{K}} = \omega_{K,\bar{K}} - \omega_0$  with

$$\omega_{K,\bar{K}} = \sqrt{m_K^2 + p^2 - a_{K,\bar{K}}\rho_s + (b_K\rho_B^{\text{net}})^2} \pm b_K\rho_B^{\text{net}} \quad (2)$$

and  $\omega_0 = \sqrt{m_K^2 + p^2}$ , where  $m_K$  is the kaon mass, and the values of  $a_K$ ,  $a_{\bar{K}}$ , and  $b_K$  can be found in Ref. [28]. In the above,  $\rho_s$  is the scalar density and is calculated self-consistently in terms of the effective quark and antiquark masses determined from the same relativistic mean-field model of Ref. [27] and  $\rho_B^{\text{net}} = \rho_B - \rho_{\bar{B}}$  is the net baryon density. The "+" and "-" signs are for kaons and antikaons, respectively.

The pion potentials are related to their self-energies  $\Pi_s^{\pm 0}$  according to  $U_{\pi^{\pm 0}} = \Pi_s^{\pm 0}/(2m_\pi)$ , where  $m_\pi$  is the pion mass. Only contributions from the pion-nucleon  $s$ -wave interaction to the pion self-energy were included in our study, and they have been calculated up to the two-loop order in the chiral perturbation theory [29]. In asymmetric nuclear matter of proton density  $\rho_p$  and neutron density  $\rho_n$ , the resulting  $\pi^-$  and  $\pi^+$  self-energies are given, respectively, by

$$\begin{aligned} \Pi_s^-(\rho_p, \rho_n) &= \rho_n[T_{\pi N}^- - T_{\pi N}^+] - \rho_p[T_{\pi N}^- + T_{\pi N}^+] \\ &\quad + \Pi_{\text{rel}}^-(\rho_p, \rho_n) + \Pi_{\text{cor}}^-(\rho_p, \rho_n), \\ \Pi_s^+(\rho_p, \rho_n) &= \Pi_s^-(\rho_n, \rho_p). \end{aligned} \quad (3)$$

In the above,  $T^+$  and  $T^-$  are, respectively, the isospin-even and isospin-odd  $\pi N$   $s$ -wave scattering  $T$ -matrices, which are given by the one-loop contribution in chiral perturbation theory;  $\Pi_{\text{rel}}^-$  is due to the relativistic correction; and  $\Pi_{\text{cor}}^-$  is the contribution from the two-loop

order in the chiral perturbation theory. Their expressions can be found in Ref. [29].

For nucleon and strange baryon resonances in a hadronic matter, we simply extend the above result by treating them as neutron- or proton-like baryons according to their isospin structure [26] and light quark numbers.

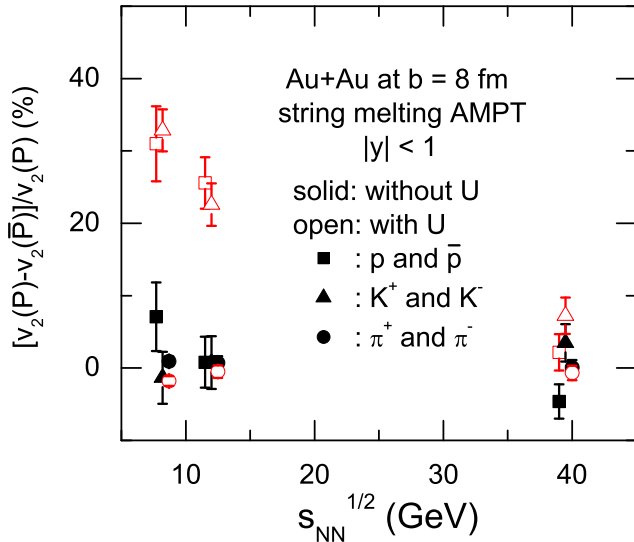


FIG. 1: (Color online) Relative elliptic flow difference between protons and antiprotons,  $K^+$  and  $K^-$ , and  $\pi^+$  and  $\pi^-$  with and without hadronic mean-field potentials in Au+Au collisions at  $\sqrt{s_{NN}} = 7.7, 11.5,$  and  $39$  GeV and impact parameter  $b = 8$  fm. Taken from Ref. [16].

The mean-field potentials are included in the ART model by using the test particle method [30]. For the parton scattering cross section in ZPC and the ending time of the partonic phase, they are determined from fitting the measured charged particle  $v_2$  and freeze-out energy density calculated from the extracted baryon chemical potential and temperature at chemical freeze-out [31]. The resulting relative  $p_T$ -integrated elliptic flow difference between particles and their antiparticles at midrapidity ( $|y| < 1$ ) are shown in Fig. 1. It is seen that without hadronic mean-field potentials, the relative  $v_2$  splitting is very small as expected. In the baryon-rich and neutron-rich matter formed in Au+Au collisions at BES energies, the hadronic potential is slightly attractive for nucleons, deeply attractive for antinucleons, slightly repulsive for  $K^+$ , deeply attractive for  $K^-$ , slightly repulsive for  $\pi^-$ , and slightly attractive for  $\pi^+$ . Figure 1 shows that the sign of the relative  $v_2$  splitting is consistent with that expected from the different hadronic mean-field potentials for particles and their antiparticles. Also, the  $v_2$  difference decreases with increasing beam energy. These results are qualitatively consistent with the experimentally measured values of about 63% and 13% at 7.7 GeV, 44% and 3% at 11.5 GeV, and 12% and 1% at 39 GeV for

the relative  $v_2$  difference between  $p$  and  $\bar{p}$  and between  $K^+$  and  $K^-$ , respectively [9]. Similar to the experimental data, the relative  $v_2$  difference between  $\pi^+$  and  $\pi^-$  is negative at all energies after including their potentials, although ours have a smaller magnitude.

#### IV. EFFECTS OF PARTONIC POTENTIALS

To include mean-field potentials for  $u, d,$  and  $s$  quarks and their antiquarks in the partonic phase, we have developed a partonic transport model based on the NJL model [17]. The Lagrangian of the 3-flavor NJL model is given by [7]

$$\begin{aligned} \mathcal{L} = & \bar{\psi}(i \not{\partial} - M)\psi + \frac{G}{2} \sum_{a=0}^8 \left[ (\bar{\psi} \lambda^a \psi)^2 + (\bar{\psi} i \gamma_5 \lambda^a \psi)^2 \right] \\ & + \sum_{a=0}^8 \left[ \frac{G_V}{2} (\bar{\psi} \gamma_\mu \lambda^a \psi)^2 + \frac{G_A}{2} (\bar{\psi} \gamma_\mu \gamma_5 \lambda^a \psi)^2 \right] \\ & - K \left[ \det_f \left( \bar{\psi} (1 + \gamma_5) \psi \right) + \det_f \left( \bar{\psi} (1 - \gamma_5) \psi \right) \right], \quad (4) \end{aligned}$$

with the quark field  $\psi = (\psi_u, \psi_d, \psi_s)^T$ , the current quark mass matrix  $M = \text{diag}(m_u, m_d, m_s)$ , and the Gell-Mann matrices  $\lambda^a$  in  $SU(3)$  flavor space. In the case that the vector and axial-vector interactions are generated by the Fierz transformation of the scalar and pseudo-scalar interactions, their coupling strengths are given by  $G_V = G_A = G/2$ , while  $G_V = 1.1G$  was used in Ref. [32] to give a better description of the vector meson mass spectrum calculated from the NJL model. Other parameters like  $m_u, m_d, m_s, G,$  and  $K$  are taken from Refs. [7, 32]. In the mean-field approximation, the above Lagrangian leads to an attractive scalar mean-field potential for both quarks and antiquarks. With a nonvanishing  $G_V$ , it further gives rise to a repulsive vector mean-field potential for quarks but an attractive one for antiquarks in a baryon-rich quark matter.

For the initial parton distributions, they are taken from the HIJING subroutine in the AMPT model. The parton scattering cross section is determined by fitting the measured  $v_2$  of final charged particles. Again the test particle method is used in the NJL transport model, and discrete lattices for space are used to calculate the local density and potential. The evolution of the partonic phase ends when the energy density of the central cell decreases to about  $0.8 \text{ GeV}/\text{fm}^3$  that is expected for the quark to hadron phase transition. The quark matter is then converted to hadrons by the coalescence model of Refs. [33, 34] with the probability for a quark and an antiquark to form a meson given by the quark Wigner function of the meson, while the probability for three quarks or antiquarks to coalesce to a baryon or an antibaryon given by the quark Wigner function of the baryon or antibaryon. The relative  $v_2$  difference between resulting  $p$  and  $\bar{p}$ ,  $\Lambda$  and  $\bar{\Lambda}$ , and  $K^+$  and  $K^-$  is given in Fig. 2 as

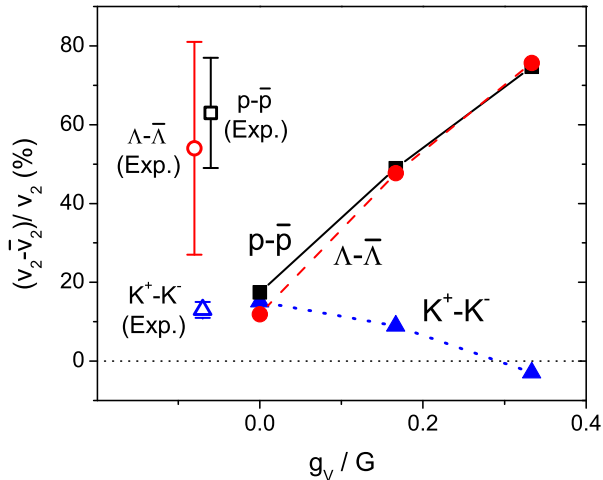


FIG. 2: (Color online) Relative elliptic flow difference between protons and antiprotons,  $K^+$  and  $K^-$ , and  $\Lambda$  and  $\bar{\Lambda}$  as a function of the ratio of the partonic vector coupling constant to the scalar one in Au+Au collisions at  $\sqrt{s_{NN}} = 7.7$  GeV with impact parameter  $b = 8$  fm. The experimental data are taken from Ref. [9]. Taken from Ref. [20].

a function of the ratio of the partonic vector coupling constant to the scalar one in the NJL model, and the experimental results from Ref. [9] are also shown for comparison. Without vector potential, i.e.,  $g_v = \frac{2}{3}G_V = 0$ , there is already slightly  $v_2$  splitting between particles and their antiparticles, and this is due to the slightly larger quark than antiquark  $v_2$  as a result of a smaller initial spatial eccentricity for quarks than for produced antiquarks. With increasing  $g_v$ , the difference between proton and antiproton  $v_2$  also increases because of the increasing difference of light quark and antiquark  $v_2$  due to a less attractive potential for quarks than for antiquarks. Similarly, the relative  $v_2$  difference between  $\Lambda$  and  $\bar{\Lambda}$  increases with increasing  $g_v$ . On the other hand, the relative  $v_2$  difference between  $K^+$  and  $K^-$  becomes smaller or even negative for large values of  $g_v$ . This is because the vector mean field, which acts similarly on light and strange (anti-)quarks, leads to a smaller antis-trange than strange quark  $v_2$  and also reduces the effect due to different spatial eccentricities of quarks and antiquarks. For pions, since the potentials for  $u$  and  $d$  quarks are the same in the present 3-flavor NJL model due to the neglect of isovector coupling between quarks and antiquarks, there is no  $v_2$  difference between  $\pi^+$  and  $\pi^-$ .

## V. EFFECTS OF BOTH HADRONIC AND PARTONIC POTENTIALS

With only hadronic potentials, Figure 1 shows that our results slightly underestimate the  $v_2$  splitting between  $p$  and  $\bar{p}$  and overestimate that between  $K^+$  and  $K^-$  in the

experimental data. Comparing the results in Fig. 2 obtained with only partonic potentials with the experimental data, the relative  $v_2$  difference between protons and antiprotons is still underestimated, while that between  $K^+$  and  $K^-$  has a wrong sign. If the effects from the mean-field potentials on  $v_2$  in the partonic phase and the hadronic phase are additive, one would expect that the relative  $v_2$  splitting between protons and antiprotons as well as that between  $K^+$  and  $K^-$  can be quantitatively explained with both partonic and hadronic potentials for a certain value of the vector coupling constant in the NJL model. This is indeed the case as shown in Ref. [18] by replacing the ZPC model in the AMPT model with the NJL transport model and ending the partonic evolution when the effective mass of light quarks in the central cell increases to about 200 MeV when the chiral symmetry is largely broken, as well as including the hadronic mean-field potentials in the ART model.

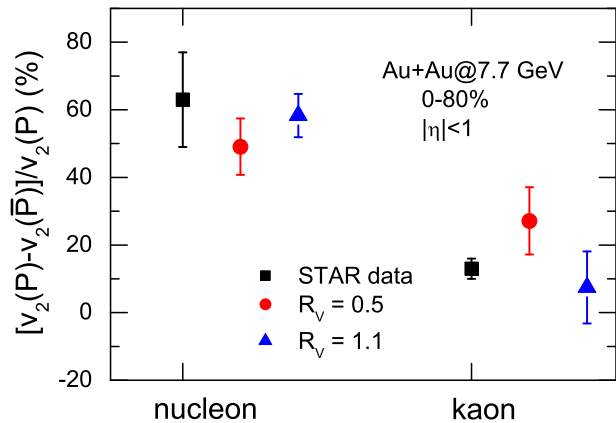


FIG. 3: (Color online) Relative elliptic flow difference between protons and antiprotons as well as between  $K^+$  and  $K^-$  using two different values for the ratio  $R_V$  of the partonic vector to scalar coupling constants in mini-bias Au+Au collisions at  $\sqrt{s_{NN}} = 7.7$  GeV. The experimental data are taken from Ref. [9]. Taken from Ref. [18].

The relative  $v_2$  difference between protons and antiprotons as well as that between  $K^+$  and  $K^-$  at midpseudorapidity ( $|\eta| < 1$ ) in mini-bias Au+Au collisions at  $\sqrt{s_{NN}} = 7.7$  in this more complete study are shown in Fig. 3 for two values of  $R_V = G_V/G = 0.5$  and 1.1. The experimental data from the STAR Collaboration [9], which are shown by filled squares, can now be quantitatively reproduced with both  $R_V = 0.5$  and  $R_V = 1.1$  within the statistical error. Also, we have found that with increasing value of  $R_V$  the relative  $v_2$  difference between protons and antiprotons increases, while that between  $K^+$  and  $K^-$  decreases. It is thus expected that further reducing the value of  $R_V$  would underestimate the relative  $v_2$  difference between protons and antipro-

tons and overestimate that between  $K^+$  and  $K^-$ , while further increasing the value of  $R_V$  would underestimate that between  $K^+$  and  $K^-$ . To reproduce both the relative  $v_2$  differences between protons and antiprotons as well as that between  $K^+$  and  $K^-$  requires the value of  $R_V$  to be about  $0.8 \pm 0.3$ .

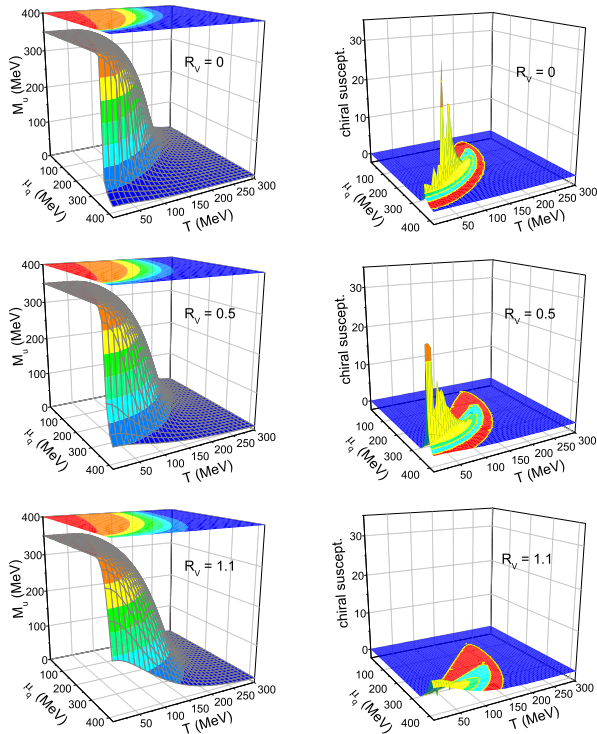


FIG. 4: (Color online) The dynamical light quark mass (left) and the corresponding susceptibility (right) in the  $(\mu_q, T)$  plane from different relative vector coupling constant  $R_V = G_V/G$ .

According to Refs. [4–7], the value of the vector coupling would affect the location of the critical point in the QCD phase diagram and thus the QCD phase structure. In Fig. 4 we display the dynamical light quark mass, which is a function of the quark condensate [17], and the corresponding susceptibility, which is defined as the derivative of the dynamical quark mass with respect to the quark chemical potential. One sees that at smaller values of quark chemical potential  $\mu_q$  and temperature  $T$ , the dynamical quark mass is large, corresponding to the phase where chiral symmetry is broken. For larger values of  $\mu_q$  or  $T$ , the dynamical quark mass is similar to the current quark mass, corresponding to the phase where chiral symmetry is restored. A smooth change from the first phase to the second phase represents a cross-over chiral phase transition, while a sudden change represents a first-order phase transition. The critical point is exactly where the cross-over transition changes to a first-order one. One sees from the susceptibility that the critical point moves to lower temperatures with increasing vector coupling constant, similar to that observed in Refs. [4–

7]. This is not surprising because the equation of state of baryon-rich matter becomes stiff with larger values of  $G_V$ , so that the phase transition is more likely to be a crossover rather than a first-order one.

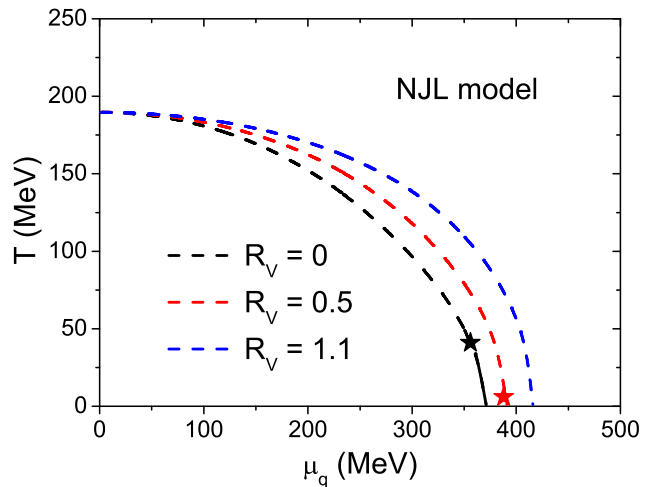


FIG. 5: (Color online) The chiral phase boundary and the corresponding critical point (labeled as stars) based on the Nambu-Jona-Lasinio model in the  $(\mu_q, T)$  plane from different relative vector coupling constant  $R_V = G_V/G$ .

Defining the phase boundary where the chiral condensate is half of the value at  $(\mu_q = 0, T = 0)$  as the phase boundary [5], the phase diagram with chiral phase transition with different  $R_V$  is shown in Fig. 5. One should keep in mind that the phase boundary is only accurate for the first-order phase transition but is artificially defined for a crossover, as shown by the dashed lines in Fig. 5. It is thus clearly seen that based on the same NJL Lagrangian from the transport model study and the phase diagram calculation, the constraint of the vector coupling  $R_V = 0.5 \sim 1.1$  leads to the conclusion that the critical point may disappear or is located at extremely low temperatures.

The above NJL Lagrangian only includes the contribution of quarks and antiquarks and can not describe the deconfinement phase transition. In Ref. [35] K. Fukushima included the Polyakov loop representing the gluon contribution, and the Polyakov loop can be taken as the order parameter of the deconfinement phase transition [36]. The Polyakov-looped Nambu-Jona-Lasinio (pNJL) model is identical to the NJL model at zero temperature but has an additional thermal potential at finite temperature [5]

$$\Omega_{\text{Polyakov}} = -b \cdot T \{ 54e^{-a/T} \bar{l} \bar{l} + \ln[1 - 6\bar{l} - 3(\bar{l}\bar{l})^2 + 4(l^3 + \bar{l}^3)] \}, \quad (5)$$

where the parameters  $a$  and  $b$  are fitted to make the quark condensate and the Polyakov loop  $l$  cross each other at about  $T = 200$  MeV at zero quark chemical potential [5]. The phase structure with the contribution of

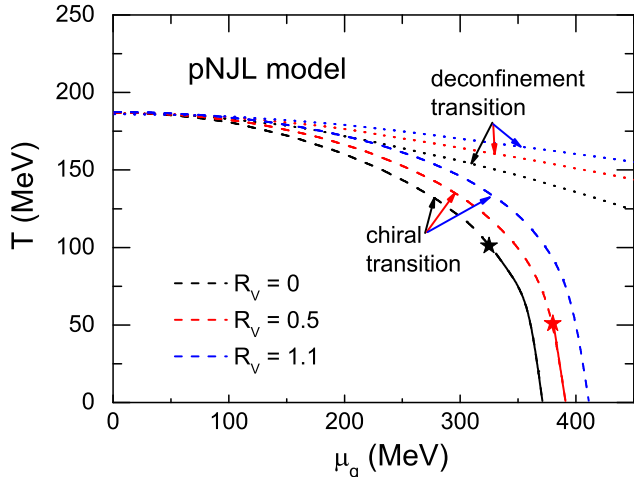


FIG. 6: (Color online) The chiral phase boundary, the corresponding critical point (labeled as stars), and the deconfinement phase boundary based on the Polyakov-looped Nambu-Jona-Lasinio model in the  $(\mu_q, T)$  plane from different relative vector coupling constant  $R_V = G_V/G$ .

the polyakov loop is displayed in Fig. 6, where the deconfinement phase boundary is defined as  $l = 1/2$  [5]. The deconfinement transition is always a crossover as a result of finite dynamical quark mass in the pNJL model. On the other hand, the critical point moves to higher temperatures after including the polyakov loop, as already discussed in Ref. [5]. However, the conclusion that the critical point disappears or is located at lower temperatures with larger values of  $R_V$  doesn't change even with the inclusion of the polyakov loop. It would be of great interest to include gluon contribution in both the transport model study and the phase diagram calculation in the future study.

## VI. CONCLUSIONS AND OUTLOOK

We have reviewed our recent studies on the effects of mean-field potentials on the elliptic flow splitting between particles and their antiparticles in the beam-energy scan program at RHIC. By including the hadronic mean-field potentials in the ART model of a multiphase transport model, the  $v_2$  splitting is qualitatively consistent with the experimental results, while the magnitude of the relative  $v_2$  difference between protons and antipro-

tons as well as  $\pi^+$  and  $\pi^-$  are underestimated, and that between  $K^+$  and  $K^-$  is overestimated. With only partonic potentials from a 3-flavor NJL transport model, the relative  $v_2$  difference between protons and antiprotons is still underestimated while that between  $K^+$  and  $K^-$  has a wrong sign when these hadrons are produced from the coalescence of quarks and antiquarks. Including both the partonic and hadronic potentials in the AMPT model, the relative  $v_2$  difference between protons and antiprotons as well as that between  $K^+$  and  $K^-$  can be quantitatively reproduced, and this further helps to constrain the  $R_V = G_V/G$  in the NJL model to about  $R_V = 0.8 \pm 0.3$ . Based on the NJL Lagrangian used in the transport model study, we have further calculated the corresponding phase diagram and found that the resulting critical point in the chiral phase transition disappears or is located at very low temperatures based on the obtained constraint of  $R_V$ , and the conclusion remains the same even if the contribution of Polyakov loop to the thermal potential is taken into account.

In the previous studies, we have only reproduced the relative  $v_2$  difference in mini-bias Au+Au collisions at  $\sqrt{s_{NN}} = 7.7$  GeV. It will be interesting to study the  $v_2$  splitting at higher energies as this would provide the possibility of studying the net baryon or baryon chemical potential dependence of  $R_V$ . In addition, since the partonic phase is more important in mid-central collisions than in peripheral collisions, it will also be of interest to study the centrality dependence of the  $v_2$  splitting to further constrain the parameters in our model. Since the location of the QCD critical point is sensitive to the value of  $R_V$ , further investigations on the  $v_2$  splitting in the baryon-rich matter can help map out the QCD phase structure.

## Acknowledgments

This work was supported by the National Key Basic Research Program of China (973 Program) under Contract Nos. 2015CB856904 and 2014CB845401, the "Shanghai Pujiang Program" under Grant No. 13PJ1410600, the "100-talent plan" of Shanghai Institute of Applied Physics under Grant No. Y290061011 from the Chinese Academy of Sciences, the National Natural Science Foundation of China under Grant No. 11475243, the US National Science Foundation under Grant No. PHY-1068572, and the Welch Foundation under Grant No. A-1358.

[1] BERNARD C, BURCH T, DETAR C *et al.* (MILC Collaboration). Phys Rev D, 2005, **71**: 034504.  
 [2] AOKI Y, ENDRODI G, FODOR Z *et al.* Nature, 2006, **443**: 675.

[3] BAZAVOV A, BHATTACHARYA T, CHENG M *et al.* Phys Rev D, 2012, **85**: 054503.  
 [4] ASAKAWA M and YAZAKI K. Nucl Phys A, 1989, **504**: 668.

- [5] FUKUSHIMA K. Phys Rev D, 2008, **77**: 114028 [Erratum-ibid. D, 2008, **78**: 039902].
- [6] CARIGNANO S, NICKEL D, and BUBALLA M. Phys Rev D, 2010, **82**: 054009.
- [7] BRATOVIC N M, HATSUDA T, and WEISE W. Phys Lett B, 2013, **719**: 131.
- [8] KUMAR L (STAR Collaboration). J Phys G, 2011, **38**: 124145.
- [9] MOHANTY B (STAR Collaboration). J Phys G, 2011, **38**: 124023.
- [10] STAR Collaboration. Phys Rev Lett, 2013, **110**: 142301.
- [11] STAR Collaboration. Phys Rev Lett, 2007, **98**: 162301.
- [12] BURNIER Y, KHARZEEV D E, LIAO J, and YEE H U. Phys Rev Lett, 2011, **107**: 052303.
- [13] DUNLOP J C, LISA M A, and SORENSEN P. Phys Rev C, 2011, **84**: 044914.
- [14] GRECO V, MITROVSKI M, and TORRIERI G. Phys Rev C, 2012, **86**: 044905.
- [15] STEINHEIMER J, KOCH V, and BLEICHER M. Phys Rev C, 2012, **86**: 044903.
- [16] XU J, CHEN L W, KO C M, and LIN Z W. Phys Rev C, 2012, **85**: 041901.
- [17] SONG T, PLUMARI S, GRECO V, KO C M, and LI F. Nucl Phys A, arXiv: 1211.5511 [nucl-th].
- [18] XU J, SONG T, KO C M, and LI F. Phys Rev Lett, 2014, **112**: 012301.
- [19] KO C M, CHEN L W, GRECO V, LI F, LIN Z W, PLUMARI S, SONG T, and XU J. Nucl Sci Tech, 2013, **24**: 050525.
- [20] KO C M, CHEN L W, GRECO V, LI F, LIN Z W, PLUMARI S, SONG T, and XU J. Acta Phys Polon Supp, 2014, **7**: 183.
- [21] DANIELEWICZ P, LACEY R, and LYNCH W G. Science, 2002, **298**: 1592.
- [22] LIN Z W, KO C M, LI B A, ZHANG B, and PAL S. Phys Rev C, 2005, **72**: 064901.
- [23] XU J and KO C M. Phys Rev C, 2011, **83**: 021903 (R); 2011, **83**: 034904; 2011, **84**: 014903; 2011, **84**: 044907.
- [24] WANG X N and GYULASSY M. Phys Rev D, 1991, **44**: 3501.
- [25] ZHANG B. Comp Phys Comm, 1998, **109**: 193.
- [26] LI B A and KO C M. Phys Rev C, 1995, **52**: 2037.
- [27] LI G Q, KO C M, FANG X S, and ZHENG Y M. Phys Rev C, 1994, **49**: 1139.
- [28] LI G Q, LEE C H, and BROWN G E. Phys Rev Lett, 1997, **79**: 5214; Nucl Phys A, 1997, **625**: 372.
- [29] KAISER N and WEISE W. Phys Lett B, 2001, **512**: 283.
- [30] WONG C Y. Phys Rev C, 1982, **25**: 1460.
- [31] ANDRONICA A, BRAUN-MUNZINGERA P, and STACHEL J. Nucl Phys A, 2010, **834**: 237c.
- [32] LUTZ M F M, KLIMT S, and WEISE W. Nucl Phys A, 1992, **542**, 521.
- [33] GRECO V, KO C M, and LEVAI P. Phys Rev Lett, 2003, **90**: 202302; Phys Rev C, 2003, **68**: 034904.
- [34] CHEN L W, KO C M, and LI B A. Phys Rev C, 2003, **68**: 017601; Nucl Phys A, 2003, **729**: 809.
- [35] FUKUSHIMA K. Phys Lett B, 2004, **591**: 277.
- [36] FUKUSHIMA K and HATSUDA T. Rep Prog Phys, 2011, **74**: 014001.